

## Bifurcation into shear bands on the Bishop and Hill polyhedron. Part II: Case of the vertices

M. DARRIEULAT<sup>(1)</sup>, D. CHAPELLE<sup>(2)</sup>

<sup>(1)</sup> *SMS, R3M, UMR CNRS 5146,  
Ecole Nationale Supérieure des Mines de Saint-Etienne,  
158 cours Fauriel, 42023 Saint-Etienne cedex 2, France.*

<sup>(2)</sup> *LMARC, Institut FEMTO ST, UMR CNRS 6174,  
24 rue de l'Épitaphe,  
25000 Besançon, France.*

THE PRESENT PAPER is the second of a series of three papers devoted to the micro-mechanical conditions which render possible the appearance of shear bands in crystalline materials. It focuses on the deformation at the vertices of the Bishop and Hill polyhedron, which are important because most of the shear bands originate at the grain boundaries where many slip systems are active. The conditions of bifurcation are analysed on the scale of the slip systems by crystallographic class of vertices. An application is given in the case of channel-die compression and it shows that the texture components are unequally liable to shear banding, the Copper one, for example, being more sensitive than Goss, as known experimentally. There is also a good agreement of the predictions with the geometry of the bands, especially the characteristic feature of the inclination at  $35^\circ$  with respect to the rolling axis. Considerations follow on the actual implementation, by micro-structural phenomena, of the localization whose mechanical possibility has been discussed in the article.

**Key words:** shear bands, channel-die compression, bifurcation, vertex.

### Notations

$h, k, l, u, v, w$	Miller–Bravais indices,
$a, b, c, l, m, l$	specific Miller–Bravais indices,
$\theta_1, \theta_2$	angles determining the normal to a shear plane in the axes of the crystal,
$\phi_1, \Phi, \phi_2$	Bunge angles,
$\sigma$	uniaxial Cauchy stress component,
$\langle M \rangle$	average Taylor factor,
$H_a$	macroscopic strain hardening modulus,
$\bar{\epsilon}$	Mises-type equivalent strain,
$\dot{\epsilon}$	uniaxial strain rate,
$\gamma$	accumulated plastic strain,

$\psi_1, \psi_2$	angles made by the normal to a shear plane with the axes of the channel die,
RD	rolling direction,
TD	transverse direction,
ND	normal direction.

## 1. Introduction

A GENERAL THEORY of the bifurcation into shear bands of rate-insensitive, ductile f.c.c. single crystals with uniform strain hardening obeying the Schmid law has been proposed in a previous article [1]. It was shown that the conditions which determine the possibility of the bifurcation form a system ( $S$ ) of nine equations, labelled Eqs. (3.9)<sub>1</sub> to (3.9)<sub>9</sub> in [1]. They take different forms according to the variety activated on the Bishop and Hill polyhedron. The present paper deals with the case of the vertices, which form five crystallographic classes labelled 4A to 4E. Their importance in localization phenomena has been pointed out by various authors [2] who showed, for example, that necking in biaxial stretching can be predicted when the vertices are present on the yield locus, whereas it cannot be done in the case of a smooth flow surface. This phenomenon is called ‘vertex softening’.

The vertices of the Bishop and Hill polyhedron are particularly relevant for the study of intragranular shear banding in polycrystals since:

- i) Electron microscopy investigations show that shear bands often originate at the grain boundaries [3] where the flow is highly constrained and at least five slip systems are required to accommodate the deformation.
- ii) The question: how many slip systems are active at the centre of the grains? – has no unique answer [4], but if the Taylor hypothesis [5] is used to calculate the mechanical behaviour of a polycrystal, all the grains deform with the same completely imposed strain tensor and their deviatoric stress states correspond to the vertices of the Bishop and Hill polyhedron.

Six or eight slip systems are available according to the class of vertices, and no unique combination of glide rates produces the required strain. Nevertheless, as seen below, the onset of shear banding is uniquely determined by the present theory in terms of the ratio  $R = h_a/\tau_c$  (microscopic work hardening modulus versus critical resolved shear stress), while uncertainty remains on which systems are active in the shear band. Table 1 gives five examples of the vertices  $\mathbf{S}^v$   $v = 1..56$  of the polyhedron, one in each crystallographic class [6].

The second section of the present paper develops the bifurcation criterion for the system ( $S$ ) specified to the vertices. The task is here easier than on the edges, since here ( $S$ ) is linear with respect to all its nine unknowns. The third section contains calculations in the case of the channel-die compression, as an illustration of the previous one. The fourth one discusses the physics which supports the mechanical analysis.

**Table 1. States of deviatoric stress at various vertices of the Bishop and Hill polyhedron.**

Class 4A, vertex 1 (8 slip systems):      Class 4D, vertex 21 (6 slip systems):

$$[s_{ij}^1] = \frac{2\sqrt{6}}{3} \begin{bmatrix} 1/2 & 0 & 0 \\ 0 & 1/2 & 0 \\ 0 & 0 & -1 \end{bmatrix} \quad [s_{ij}^{21}] = \frac{\sqrt{6}}{3} \begin{bmatrix} -1/2 & 0 & 3/2 \\ 0 & -1/2 & 3/2 \\ 3/2 & 3/2 & 1 \end{bmatrix}$$

Class 4B, vertex 28 (6 slip systems):      Class 4E, vertex 7 (8 slip systems):

$$[s_{ij}^{28}] = \frac{\sqrt{6}}{2} \begin{bmatrix} 0 & 1 & 1 \\ 1 & 0 & 1 \\ 1 & 1 & 0 \end{bmatrix} \quad [s_{ij}^7] = \frac{\sqrt{6}}{2} \begin{bmatrix} 1 & 0 & 1 \\ 0 & 0 & 0 \\ 1 & 0 & -1 \end{bmatrix}$$

Class 4C, vertex 6 (8 slip systems):

$$[s_{ij}^6] = \sqrt{6} \begin{bmatrix} 0 & 1 & 0 \\ 1 & 0 & 0 \\ 0 & 0 & 0 \end{bmatrix}$$

## 2. Analysis of the bifurcation at the vertices

### 2.1. Resolution of the system $S$

As seen previously, the rate constitutive relation at the vertex  $\mathbf{S}^v$  takes the form  $\overset{\vee}{\mathbf{S}}^* = \frac{h_a}{\tau_c^2} (S^v \otimes S^v) : \mathbf{D} = \left( \frac{h_a}{\tau_c^2} S_{ij}^v D_{ij} \right) \mathbf{S}^v$ . Under the effect of continuous flow, the yield locus deforms homothetically and the deviatoric stress increment  $\overset{\vee}{\mathbf{S}}^*$  is proportional to the applied deviatoric stress  $\mathbf{S}^v$ . The bifurcation criterion is written with the help of the quantities  $C_{ij}$  which intervene in the equilibrium equations (Eqs. (3.9)<sub>1</sub> to (3.9)<sub>3</sub> of the above quoted paper):

$$(2.1) \quad C_{ij} = R S_{ik}^v S_{jl}^v \nu_k \nu_l + \frac{1}{2} \left[ S_{ik}^v \nu_j \nu_k + \delta_{ij} S_{kl}^v \nu_k \nu_l - S_{jk}^v \nu_i \nu_k - S_{ij}^v \right]$$

with  $R = h_a/\tau_c$ . Bifurcation occurs if:

$$(2.2) \quad \Delta_v = \begin{vmatrix} C_{11} & C_{12} & C_{13} & \nu_1 \\ C_{21} & C_{22} & C_{23} & \nu_2 \\ C_{31} & C_{32} & C_{33} & \nu_3 \\ \nu_1 & \nu_2 & \nu_3 & 0 \end{vmatrix} = 0.$$

The resolution of the system ( $S$ ) is split into two steps:

- i) determination of the velocity field  $\eta_i$   $i = 1..3$  in the shear band with Eqs. (3.9)<sub>1</sub> to (3.9)<sub>4</sub> of the previous paper. Due to the linearity of ( $S$ ), there

is only one possible shear direction for a given  $\nu$ . From the expression for  $\Delta_\nu$ , the bifurcation condition should *a priori* take the form of a polynomial of degree two for the unknown  $R$ . In fact, due to the particular values of the  $S_{ij}^\nu$ , it is always linear in  $R$ , and this quantity can be calculated on all the planes of the Euclidian space except in rare cases when it is infinite or undetermined. The analytical expressions of  $R$  as a function of the  $\nu_i$  vary for each vertex; e.g., if  $\nu = 1$ :

$$(2.3) \quad R = \frac{\sqrt{6}}{12} \frac{(1 - 2\nu_3^2)}{\nu_3^2 (1 - \nu_3^2)}.$$

On this specific example, it can be seen that equilibrium and normality can be satisfied by  $R$  taking any real value (the second step will put bounds on it), and that a variety of planes are possible for a given  $R$ , that is, a given state of work hardening.

- ii) the velocity field  $\eta_i$   $i = 1..3$  calculated by Eqs. (3.9)<sub>1</sub> to (3.9)<sub>4</sub> provides an admissible shear band only if it belongs to the cone of the normals of the considered vertex, that is, if the shear results of a combination of the available slip systems (plane and direction working in the required sense). For the five crystallographic classes, this implies  $R_{\min} \leq R \leq R_{\max}$  with  $R_{\min} = -R_{\max}$  as shown below.

The algorithm giving  $R$  is the following. At the vertex  $\mathbf{S}^\nu$ :

- All the planes of the Euclidian space are successively tested for bifurcation:

$$(2.4) \quad \begin{aligned} \nu_1 &= \cos \theta_1 \cos \theta_2, & 0 \leq \theta_1 < 2\pi, & & 0 \leq \theta_2 \leq \pi/2, \\ \nu_2 &= \sin \theta_1 \cos \theta_2, \\ \nu_3 &= \sin \theta_2. \end{aligned}$$

$\nu_3$  is taken positive to draw the stereographic projections.  $\theta_1$  and  $\sin \theta_2$  are varied with equal steps on the intervals  $[0, 2\pi]$  and  $[0, 1]$  respectively, to obtain an isochoric repartition [7].

- The shear flow is calculated as  $\mathbf{D} = \frac{1}{2}(\eta \otimes \nu + \nu \otimes \eta)$ .  $\eta$  is only known within a scaling factor, so that it can be taken such as  $\eta_i$ ,  $\eta_i = 1$ . Its sign is determined by the inequality  $\mathbf{S}^\nu : \mathbf{D} > 0$ . Following Bishop and Hill,  $\mathbf{D}$  belongs to the cone of the normals to the vertex  $\mathbf{S}^{\nu_0}$  if  $\forall \nu \neq \nu_0 \quad \mathbf{S}^\nu : \mathbf{D} \leq \mathbf{S}^{\nu_0} : \mathbf{D}$ .

In the conditions on the flow cone,  $\nu$  and  $\eta$  play a symmetric role. It is not so with the equilibrium equations, which involve the spin rate  $\Omega$ . These can be written with the help of the gradient  $\mathbf{L} = \eta \otimes \nu$  of the velocity field and the rate of isostatic pressure  $\dot{p}$ :

$$(2.5) \quad \operatorname{div} \left( \frac{h_a}{\tau_c^2} (\mathbf{S}^\nu \otimes \mathbf{S}^\nu) : \mathbf{L} + \mathbf{L} \cdot \mathbf{S}^\nu - \mathbf{S}^\nu \cdot \mathbf{L} \right) - \operatorname{grad}(\dot{p}) = 0.$$

In this form, the effect of changing  $\mathbf{L}$  into  $\mathbf{L}^T$ , that is  $(hkl)[uvw]$  into  $(uvw)[hkl]$ , becomes clear. Using the properties of symmetry of the deviatoric stress tensors ( $\mathbf{S}^v \cdot \mathbf{L} = \mathbf{L}^T \cdot \mathbf{S}^v$ ) and the fact that the sign of  $\dot{p}$  is unimportant, it appears that:

- at one vertex  $\mathbf{S}^v$ ,  $\mathbf{L}$  and  $\mathbf{L}^T$  are obtained for opposite values of  $R$ ,
- at the vertices  $\mathbf{S}^v$  and  $\mathbf{S}^{v+28} = -\mathbf{S}^v$ , identical values of  $R$  correspond to transposed shear flows  $\mathbf{L}$  and  $\mathbf{L}^T$ . Hence  $R_{\min} = -R_{\max}$ .  $\mathbf{S}^v$  and  $\mathbf{S}^{v+28}$  have common  $R$  extrema which exchange the shear plane and the shear direction.

Figure 1 shows the stereographic projections of the admissible normals  $\nu$ , the (001) pole being in the centre of the projection. They have been regrouped according to the crystallographic class of the vertices. They form continuous cones, with rounded frontiers except for a few apices. The directions of the latter have been shown in the figure. Some have simple Miller indices (e.g.  $\{112\}$  for the classes 4A and 4B), some have more complex values which have been given approximately (e.g.  $\sim \{113\}$  for the class 4D). The  $l = 0.100$  and  $m = 0.258$  which, as seen below, correspond to extreme values, are found for the class 4C. Many planes can be activated from vertices of different classes, especially in the stereographic triangle delimited by  $\{101\}$ ,  $\{112\}$  and  $\{111\}$ ; but a number is unfit for all vertices, forming a cone which appears in Fig. 1f, approximately centred around the direction  $\{631\}$ .

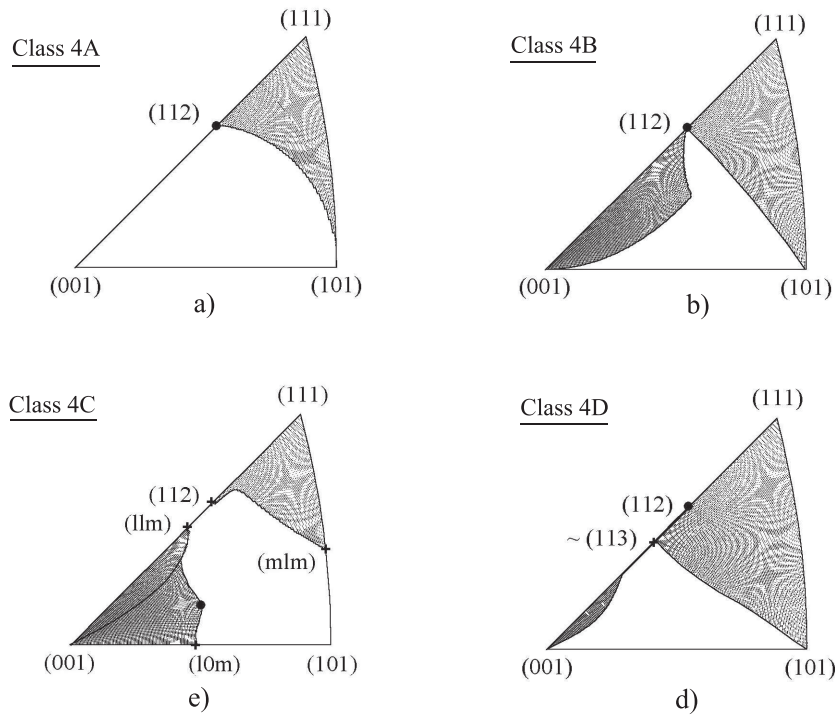


[Fig. 1]

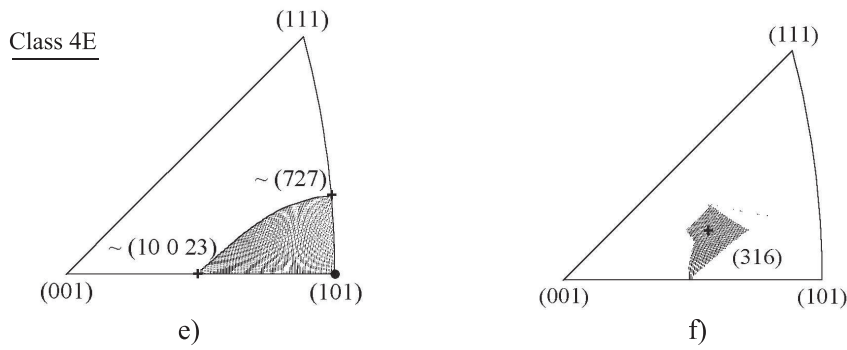


FIG. 1. (a) Class 4A; (b) Class 4B; (c) Class 4C; (d) Class 4D; (e) Class 4E; (f) planes unfit for bifurcation · extremum for  $R$  + remarkable, non extreme value for  $R$ .

The fact that the plane  $\{111\}$  is a possible shear plane for the classes 4A to 4D is especially important because, as will be discussed later, many authors think that shear bands have their origin in the coarse slip which occurs on the octahedral planes [8]. This mechanism is not possible in the class 4E.

The characteristic values of  $R$  have been regrouped in Table 2: 4B and 4D are the most favoured classes from the point of view of strain hardening. The average  $R_{av}$  is zero in the classes 4A and 4C, and has opposite values for opposite vertices in the other classes. The values  $R > 0$  correspond to positive work hardening, which means that the bifurcation is possible without detrimental effects in the material. The largely negative values of  $R$  are of no interest, since they cannot be reached without ruining the material.

**Table 2. Characteristic values of bifurcation according to the class of the vertices.**

Class	4A	4B	4C	4D	4E
$R_{max}$	$\sqrt{6}/8 = 0.306$	$7\sqrt{6}/16 = 1.071$	0.620	$7\sqrt{6}/16 = 1.071$	$\sqrt{6}/3 = 0.816$
$R_{av}$	0	$\pm 0.0679$	0	$\pm 0.1605$	$\pm 0.0426$
Percentage of bifurcating planes	5.9	15.3	26.1	4.0	3.1
Occurrence	4.1	18.1	40.9	20.1	16.8

The percentage of planes suitable for bifurcation has also been noted; its total hardly exceeds one half of all suitable planes, a fact consistent with the existence of a no shear banding spot around  $\{631\}$ . These figures have been put in relation with the results by FORTUNIER and LINHART [9], who have considered the possible plastic flow and calculated the frequency with which they activate the various vertices (line: 'Occurrence' in the Table 2).

In Figure 2, the stereographic projections of  $\nu$  and of the corresponding  $\eta$  have been represented facing each other for one vertex taken in each of the five crystallographic classes. The isovalues of  $R$  have also been reported. Such a particular shear system appears in two sub-figures, with the same graphic symbol. In the case of the classes 4A and 4C, because of the symmetry, it was only necessary to represent one quadrant of the projections of  $\nu$ . The Miller–Bravais indices and the corresponding  $R$  values of a few remarkable points are presented in Table 3.

**Table 3. Remarkable points in Fig. 2.**

Class and vertex	Point	Miller–Bravais indices	$R = h_a/\tau_c$
4A $S^1$	1	(112)[ $\bar{1}\bar{1}1$ ]	0.306
	2	(111)[ $\bar{1}\bar{1}2$ ]	-0.306
	3	(101)[10 $\bar{1}$ ]	0
	4	(011)[01 $\bar{1}$ ]	0
4B $S^{28}$	1	(100)[011]	0.204
	2	(211)[ $\bar{1}11$ ]	-1.071
	3	(011)[100]	-0.204
	4	( $\bar{1}11$ )[211]	1.071
	5	(112)[ $\bar{1}\bar{1}1$ ]	-1.071
	6	(001)[ $\bar{1}\bar{1}0$ ]	0.204
	7	( $\bar{1}\bar{1}1$ )[112]	1.071
	8	( $\bar{1}\bar{1}0$ )[001]	-0.204
	9	(121)[1 $\bar{1}1$ ]	-1.071
	10	(010)[101]	0.204
	11	(101)[010]	-0.204
	12	(1 $\bar{1}1$ )[121]	1.071
4C $S^6$	1	(100)[0 $\bar{1}0$ ]	-0.106
	2	(m10)[l $\bar{m}0$ ]	-0.520
	3	(mll)[0 $\bar{1}1$ ]	-0.317
	4	(112)[ $\bar{1}\bar{1}1$ ]	0.306
	5	(111)[ $\bar{1}\bar{1}2$ ]	-0.306
4D $S^{21}$	1	(111)[ $\bar{1}\bar{1}2$ ]	-1.071
	2	(110)[00 $\bar{1}$ ]	0.104
	3	(001)[110]	-0.204
	4	( $\bar{1}\bar{1}2$ )[111]	1.071
4E $S^7$	1	(101)[ $\bar{1}01$ ]	-0.816
	2	( $\bar{1}01$ )[101]	0.816

## 2.2. Most favoured bifurcation systems

In the results presented above, it has already been referred to the shear systems corresponding to  $R_{\max}$  which appear in Fig. 2. They are the first which allow the bifurcation from a homogeneous deformation mode while  $h_a$  is high and  $\tau_c$  is small. Their list is given in Table 4 for the vertices  $\mathbf{S}^v$   $v = 1..28$ . As it is seen above, the systems for the vertices  $v = 29..56$  are obtained by exchanging the indices of the plane and of the direction of shear. The most favoured bifurcation systems have simple Miller–Bravais indices, except for the  $\{abc\} < l\bar{m}l >$  class 4C in

**Table 4. Most favoured bifurcation systems on the vertices  $v = 1..28$  of the Bishop and Hill polyhedron  $a = 0.117$ ,  $b = 0.399$ ,  $c = 0.909$ ,  $l = 0.100$  and  $m = 0.258$ .  $a\bar{l} + bm + \bar{c}l = 0$ .**

Vertex		Normal			Glide direction				
4A	1	1	1	-1	-2	1	-1	1	
		2	1	1	-2	1	1	1	
		3	1	-1	2	-1	1	1	
		4	1	1	2	-1	-1	1	
	2	1	1	-1	-1	1	-1	1	
		2	2	1	-1	1	-1	-1	
		3	2	-1	1	1	1	-1	
		4	2	1	1	-1	1	1	
	3	1	1	-2	-1	1	1	-1	
		2	1	2	-1	-1	1	1	
		3	1	-2	1	1	1	1	
		4	1	2	1	1	-1	1	
4C	4	1	$a$	$b$	$-c$	$-1$	$m$	1	
		2	$a$	$c$	$-b$	1	1	$m$	
		3	$a$	$-b$	$c$	$-1$	$m$	1	
		4	$a$	$-c$	$b$	$-1$	1	$m$	
	5	1	$b$	$a$	$-c$	$m$	$-1$	1	
		2	$c$	$a$	$-b$	1	1	$m$	
		3	$-b$	$a$	$c$	$m$	1	1	
		4	$-c$	$a$	$b$	1	$-1$	$m$	
	6	1	$b$	$-c$	$a$	$m$	1	$-1$	
		2	$c$	$-b$	$a$	1	$m$	1	
		3	$-b$	$c$	$a$	$m$	1	1	
		4	$-c$	$b$	$a$	1	$m$	$-1$	
4E	7	1	1	0	-1	1	0	1	
		8	1	1	0	1	-1	0	1
		9	1	0	1	-1	0	1	1
		10	1	0	1	1	0	-1	1
	11	1	1	-1	0	0	-1	0	
		12	1	1	1	0	-1	1	0
		13	1	1	-2	1	1	1	1
			14	1	1	-2	-1	-1	-1
	15		1	1	2	-1	-1	1	1
	16		1	1	2	1	1	-1	1
	4D	17	1	2	-1	-1	1	1	1
		18	1	2	-1	1	-1	-1	1
19		1	2	1	-1	1	-1	1	
20		1	2	1	1	-1	1	1	
21		1	1	1	-2	1	1	1	
22		1	1	-1	-2	1	-1	1	
23		1	1	-1	2	-1	1	1	
24		1	1	1	2	-1	-1	1	
4B	25	1	1	-2	-1	1	1	1	
		2	2	-1	1	1	-1	1	
		3	1	0	1	-1	1	1	
	26	1	2	-1	1	-1	-1	1	
		2	1	-2	1	1	1	1	
		3	1	-1	2	-1	1	1	
	27	1	1	-1	-2	1	-1	1	
		2	2	-1	-1	1	1	1	
		3	1	-2	-1	-1	-1	1	
	28	1	2	1	1	-1	1	1	
		2	1	2	1	1	-1	1	
		3	1	1	2	-1	-1	1	

which the are such that  $a = 0.117$ ,  $b = 0.399$ ,  $c = 0.909$ ,  $l = 0.100$  and  $m = 0.258$ . The number of the most favoured systems is one (classes 4D and 4E), three (class 4B) or four (classes 4A and 4C). A sketch of these systems has been drawn in Fig. 3. The arrows represent the forces and torques which cause the stress state.

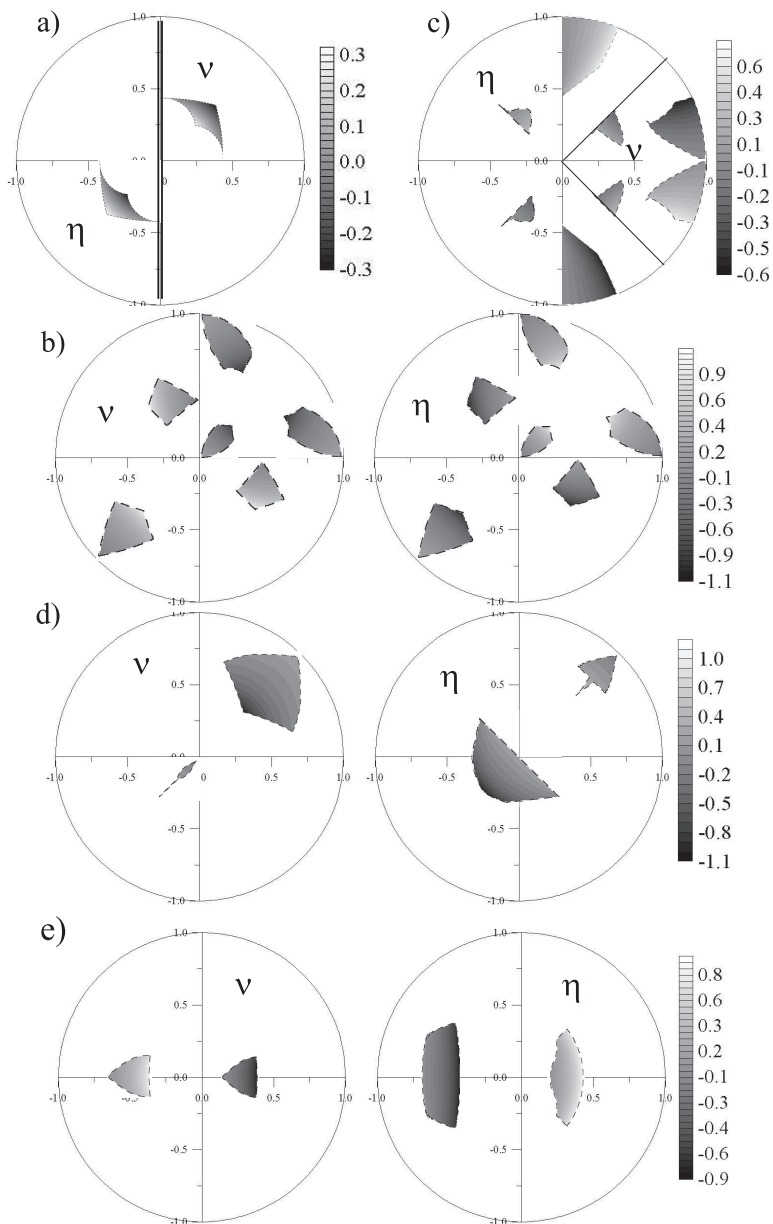
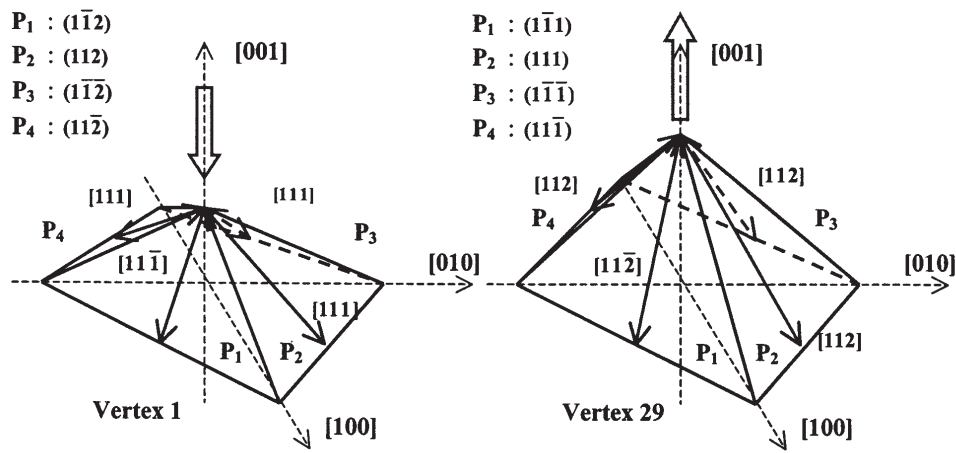


FIG. 2. Representation of the shear systems by the stereographic projections of  $\nu$  and  $\eta$  and iso-values of  $R$  (a) Class 4A; (b) Class 4B; (c) Class 4C; (d) Class 4D; (e) Class 4E.

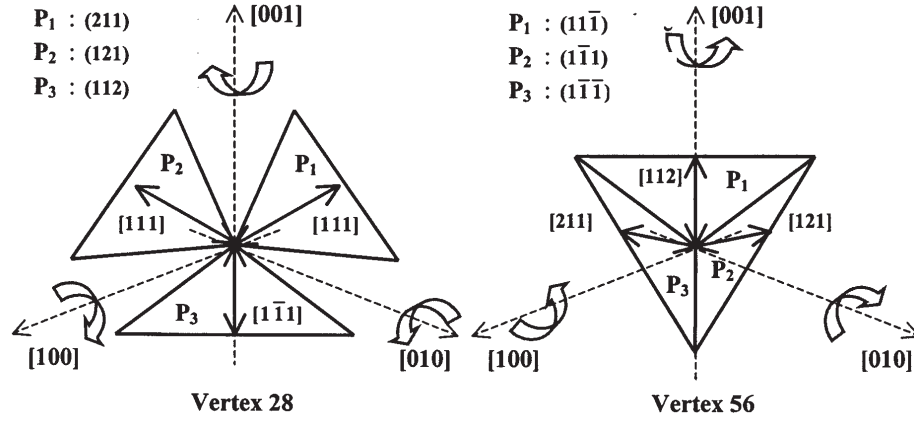
Class 4A :

- $P_1 : (1\bar{1}2)$
- $P_2 : (112)$
- $P_3 : (1\bar{1}\bar{2})$
- $P_4 : (11\bar{2})$



Class 4B :

- $P_1 : (211)$
- $P_2 : (121)$
- $P_3 : (112)$



Class 4D :

- $P_1 : (11\bar{2})$

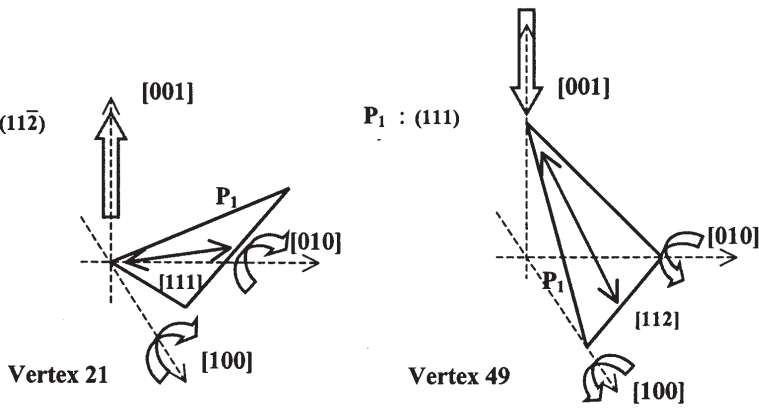
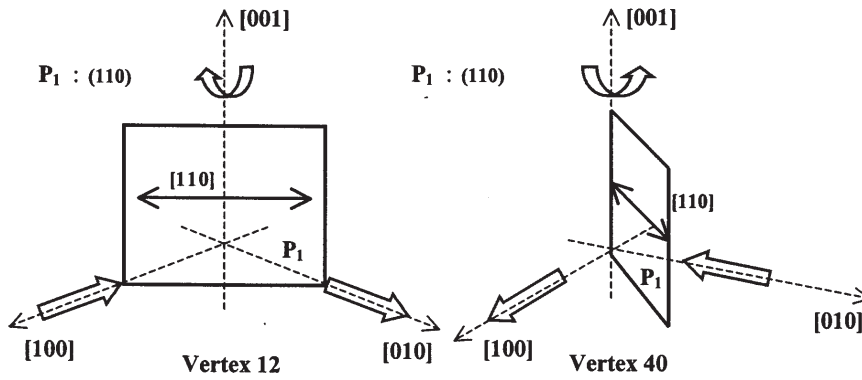


[Fig. 3]

Class 4E :



Class 4C :

- $P_1 : (ab\bar{c})$
- $P_2 : (ac\bar{b})$
- $P_3 : (a\bar{b}c)$
- $P_4 : (a\bar{c}b)$

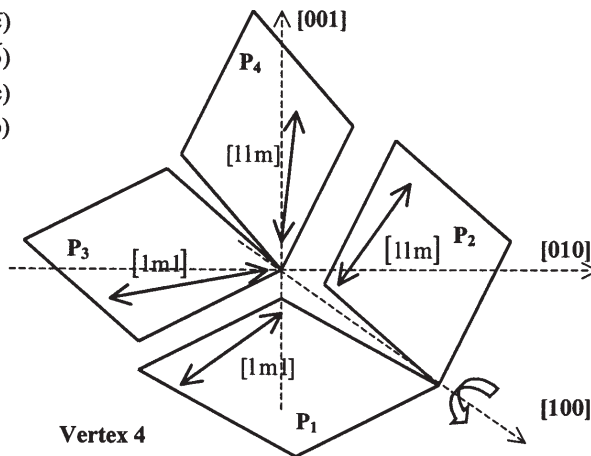


FIG. 3. Sketch of the most favoured shear systems for one vertex of each class.

The shear systems  $\{111\}\langle 112\rangle$  and  $\{110\}\langle 110\rangle$  deserve a special interest since they appear often as the most favoured slip systems and since they can be produced by the combination of two coplanar (CP) or codirectional (CD) slip systems in f.c.c. crystals. For example:

$$v = 53 \text{ (Class 4B)} \quad (111)[0\bar{1}1] + (111)[\bar{1}01] \rightarrow (111)[\bar{1}\bar{1}2],$$

$$v = 12 \text{ (Class 4E)} \quad (11\bar{1})[\bar{1}10] + (111)[\bar{1}10] \rightarrow (110)[\bar{1}10].$$

Some of these combinations (but not all) correspond to the most favoured bifurcation systems ( $R_{\max}$ ). They are by no means the only combinations of active

slip systems able to determine the flow in the shear band, but special attention is given to them because of the simplicity of the mechanism of bifurcation: the glide stops on all the slip systems except two which go on sliding with equal glide rates. Such an event may occur because, under the effect of the crystalline rotation, they become symmetrical with respect to the applied stress.

There are  $\{111\}\langle 112\rangle$  shear systems in the flow cones of all the vertices, except in the class 4E:

- For the classes 4A, 4B and 4D, they are most favoured systems at the vertices  $\mathbf{S}^v v = 29$  to 31 and 41 to 56. For the class 4A, they are not obtained as a combination of (CP) acting at the vertices. But for the class 4B ( $v = 53$  to 56), each of the three pairs of active (CP) combine with equal glide rates to give one of the most favoured slip systems. For the class 4D ( $v = 41$  to 52), one pair out of the three available ones produces a most favoured slip system.
- For the class 4C, the  $\{111\}\langle 112\rangle$  are not extreme but correspond to  $R = 0.306$  or  $R = -0.306$ .

The class 4C is especially important because of the large solid angles formed by their cones [9]. Thus, the combination of two (CP) with equal glide rates can explain 60% of the cases of the most favoured bifurcation.

### 3. The case of the channel-die compression

Shear bands form along all sorts of deformation paths, but the largest number of experimental results has been collected in rolling or by compression in a channel die, which simulates rolling [10]. A synthesis of the observations has been given by HARREN *et al.* [11]. Compared to tension, strains are much larger, the work hardening rate is always positive and there is no influence of a macroscopic localization. A distinctive feature is that the macroscopic shear bands are inclined at  $35^\circ(\pm 10\%)$  with respect to the compression plane, as in pointed out as early as in the 1910s by GROGAN, ADCOCK, ELAM and others (see MOKHTARY–DOLUI [12]).

#### 3.1. Micro-mechanical analysis

The aim of the present section is to study shear banding in channel die compression, supposing that the latter activates the vertices of the Bishop and Hill polyhedron. The axes of the appliance are labelled 1 (RD, rolling or extension direction), 2 (TD, transverse direction) and 3 (ND normal direction). When are such conditions most likely to be fulfilled?

- i) Numerous experiments have been done with single crystals. If special precautions are taken, friction is restricted [13] and the deformation can be

considered as homogeneous, at least in the bulk of the sample. The channel-die constrains three degrees of freedom (the imposed deformation rate  $D_{33}$ , and  $D_{22} = D_{23} = 0$ ).  $D_{12}$  and  $D_{13}$  are free, and can take large values [14]. Hence, the working point on the Bishop and Hill polyhedron is the edge  $d = 2$  or sometimes  $d = 1$  because of the symmetry considerations (see the third paper of the present series) rather than a vertex.

- ii) In polycrystals, especially if the texture is not strong,  $D_{12}$  and  $D_{13}$  are small, and vary in the height and the width of the sample if there is a barrelling effect. A simplified macroscopic strain rate tensor averaging these variations is:

$$(3.1) \quad \mathbf{D} = \dot{\epsilon} \begin{bmatrix} 1 & 0 & 0 \\ 0 & 0 & 0 \\ 0 & 0 & -1 \end{bmatrix}.$$

In this case, the test in the channel-die is a plane strain compression. Assuming the Taylor hypothesis, it is the strain rate tensor which will be used below for the individual grains.

If such assumptions are made, one question arises: are all the vertices  $\mathbf{S}^v$  activated in channel-die compression when all the possible crystallographic orientations are considered, and with what frequency? A test was done, varying the orientations through their Bunge angles with:  $0 \leq \phi_1 \leq \pi$ ,  $-\pi/2 \leq \Phi \leq \pi/2$ ,  $0 \leq \phi_2 \leq \pi$ . All the 56 vertices are activated, in proportions: 3.2% (4A), 12.8% (4B), 40.5% (4C), 23.1% (4D), 20.4% (4E). They do not differ much from those already referred to as the ‘Occurrence’, found in the case of the most general mechanical solicitation by FORTUNIER and LINHART [9].

### 3.2. Comparison with experimental results

The predictions of the above model can be assessed from the point of view of i) the geometry it predicts for the shear bands and ii) the deformation  $\bar{\epsilon}$  at which the bands appear. Although the grains are anisotropic, the formula  $\bar{\epsilon} = \int \left( \frac{2}{3} \dot{\epsilon}_{ij} \dot{\epsilon}_{ij} \right)^{1/2} dt$ , used by many referenced authors, is also employed in the present paper, all the more because more pertinent formulations necessitate an analytical expression for the yield surface.

There are numerous results on these two points in the literature [15, 16]. In channel die, the shear bands revealed at the surface are also found at the core of the sample, parallel to the TD axis. They form at a range of values of  $\bar{\epsilon}$  upon which it can be commented that:

- Spotting the early bands is not easy. Decorating with Lloyds’ method or depositing fiducial grids [17] show that they form earlier what was ordinary noted from scanning electron microscopy observations,

- The chemical composition of the alloy, which determines the stacking fault energy, plays a decisive role. In light alloys for example, shear bands are observed as soon as  $\bar{\varepsilon} = 0.2$  in Al-Mg systems [18]; Al-Cu offers a range of values according to the state of precipitation, solid solution or  $\theta'$  precipitates [11]; the phenomenon is postponed to large deformations in Al-Mn [14]. The present analysis discusses only the mechanical possibility of shear banding, in the case when no previous heterogeneity exists in the material.
- i) Test on the geometry of shear banding.

In the present calculation, it was assumed that the bifurcation occurs on the most favoured shear plane. Let  $\Psi_1$  be the angle (ND,  $\nu$ ) measuring the inclination of the normal to the band with respect to the compression plane and  $\Psi_2$  – the angle (RD, projection of  $\nu$  on the compression plane) giving the tilt to the plane of symmetry of the channel-die. By considering all the possible crystallographic orientations, it is possible to draw their histogram, presented by the class of vertices in Fig. 4. The three classes 4A, 4D and 4E clearly show a peak around  $\Psi_1 = 35^\circ$ , the others have a smooth maximum for this value. Such a geometry has extensively been mentioned in the literature. All the histograms in  $\Psi_2$  show a maximum around 0, which corresponds to the case when the plane of bifurcation contains the transverse direction. The number of the most favoured planes (one, three or four, according to the type of the vertices) has also been reported in Fig. 4.

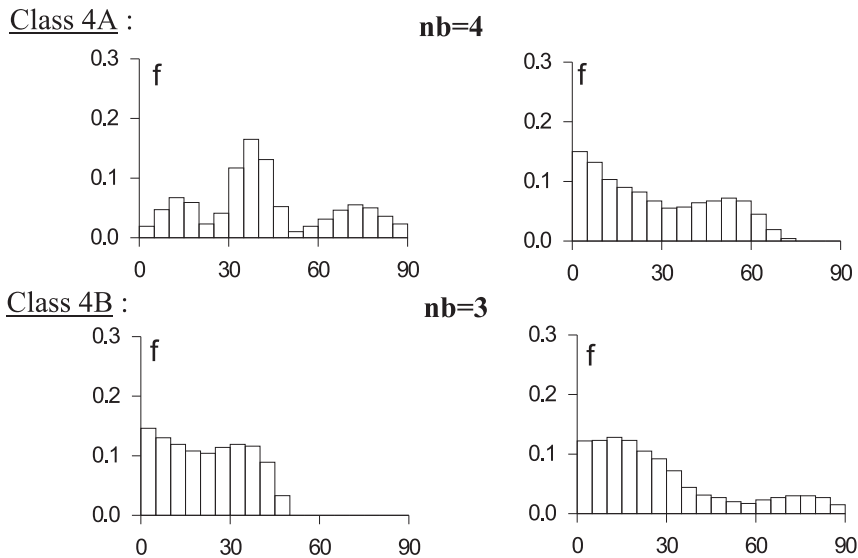


[Fig. 4]

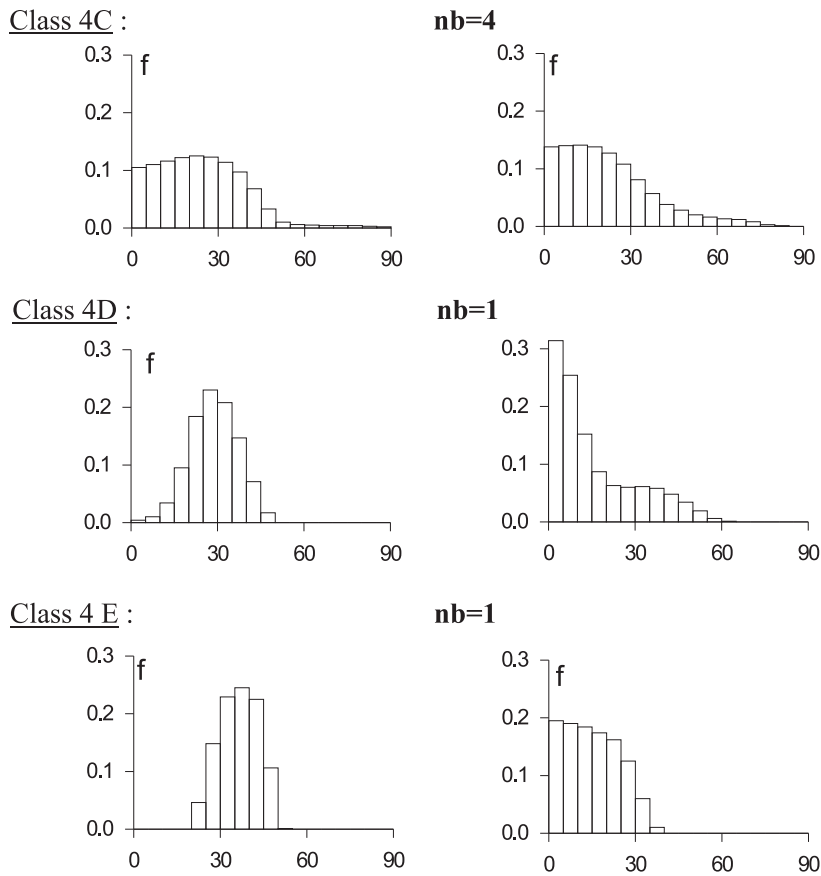


FIG. 4. Histograms of the tilts  $\Psi_1$  and  $\Psi_2$  of the most favoured shear bands Plane strain compression. **nb**: number of most favoured shear systems.

It is noteworthy that the position predicted for the most favoured bands within the grains is the position of the macroscopic shear bands. As documented by many authors, the macroscopic bands are produced by clustering of the bands formed in the individual grains. The above mechanical consideration cast a light on this phenomenon, as it shows that the most probable geometry of shear banding lies in the same range of  $\Psi_1$  and  $\Psi_2$  for all the grains.

ii) Test on the level of strain hardening at the onset of shear banding.

There is no simple transposition between  $R = h_a/\tau_c$  and the ratio  $H_a/\sigma$  which can be measured on experimental curves  $\sigma(\bar{\varepsilon})$ .  $H_a$  is the macroscopic strain hardening modulus ( $H_a = d\sigma/d\bar{\varepsilon}$ ). If  $\langle M \rangle$  is the mean Taylor factor of the grains,  $\sigma = \langle M \rangle \tau_c$  and a classical calculation gives:

$$(3.2) \quad H_a = \frac{d\sigma}{d\bar{\varepsilon}} = \langle M \rangle^2 \frac{d\tau_c}{d\gamma} + \tau_c \frac{d\langle M \rangle}{d\bar{\varepsilon}} = \langle M \rangle^2 h_a + \tau_c \frac{d\langle M \rangle}{d\bar{\varepsilon}}.$$

An evaluation of Eq. (3.2) has been done on a millimetre scale  $\{123\}\langle 634\rangle$  grain observed in the Al-4.5%Mg system [18]. Shear bands, which cannot be spotted at  $\bar{\varepsilon}=0.1$ , are clearly visible at  $\bar{\varepsilon}=0.24$ . The Taylor factor is 2.55, the applied macroscopic stress about 250 MPa,  $H_a$  is about 500 MPa, hence  $R$  is of the order of unity. This is coherent with the mechanical analysis, which predicts the activation of  $\mathbf{S}^{49}$  (class 4D), for which the above calculations give  $R=1.071$ . Similar conclusions can be drawn from [19].

On the contrary, the data collected for 99.99% aluminium show that the shear bands appear in the range  $0.2 < \bar{\varepsilon} < 0.6$ , where  $H_a$  is low (about 30 MPa) and  $R \sim 1/M^2$ ,  $M$  being the Taylor factor, that is about six times less than in the previous case. And some results in the literature are still lower:  $R \sim 0.1$  in [16].

The above calculations have been done at the grain level but, as already commented upon, full grown bands retain much of the geometry of the micro shear bands. Hence it is interesting to calculate the parameter  $R_{\max}$  for some usual rolling texture components. The latter are sets of crystallographic orientations around ideal directions which have been rendered symmetric with respect to the three planes of orthotropy of the rolled sheets. Here they have been represented by spreads of a certain angle  $\omega_0$ , so that several vertices can be activated and an average value has been taken. The spread chosen was  $5^\circ$  (the results are quite similar with  $2^\circ$  and  $10^\circ$ ). The results are regrouped by class of vertices in Table 5. The components which are the most sensitive to shear banding are T (Taylor) and Copper; then come Brass and Strange, and after them Cube; the most resistant is Goss. All this is supported by experimental results in rolling.

**Table 5. Main texture components and their most favoured bifurcation ratios.**

	Percentage of activation					Average ( $h_a/\tau_c$ ) max
	4A	4B	4C	4D	4E	
Cube $\{100\}\langle 001\rangle$	14.4	0.0	0.0	0.0	85.6	0.74
Brass $\{011\}\langle 211\rangle$	0.0	49.0	50.2	0.8	0.0	0.84
Copper $\{112\}\langle 111\rangle$	0.0	37.5	11.0	51.5	0.0	1.02
Strange $\{123\}\langle 634\rangle$	0.0	8.4	53.2	38.4	0.0	0.83
Goss $\{011\}\langle 100\rangle$	61.2	0.0	38.8	0.0	0.0	0.43
I $\{112\}\langle 110\rangle$	0.0	49.0	50.2	0.8	0.0	0.84
L $\{110\}\langle 110\rangle$	0.0	0.0	100.0	0.0	0.0	0.62
CL $\{120\}\langle 210\rangle$	2.8	0.0	78.7	0.0	18.5	0.65
CH $\{100\}\langle 120\rangle$	60.9	0.0	0.0	0.0	39.1	0.51
CG $\{210\}\langle 100\rangle$	60.9	0.0	0.0	0.0	39.1	0.51
T $\{4\ 4\ 11\}\langle 11\ 11\ 8\rangle$	0.0	35.5	1.4	63.1	0.0	1.06
E $\{111\}\langle 110\rangle$	0.0	0.0	100.0	0.0	0.0	0.62

#### 4. Main results and discussion

The bifurcation into shear bands at the vertices of the Bishop and Hill polyhedron has been studied with the help of a piecewise linear (i.e. specialized to each vertex) rate constitutive law. It shows that, when all the mechanical solicitations are considered, the shear bands can form on about one half of the planes of the Euclidean space, but not around  $\{631\}$ . For each bifurcating plane there is one shear direction and one value of the ratio  $R$ . The latter is directly linked to the deformation  $\bar{\epsilon}$  and to the work hardening.

The vertices correspond to the cases where the strain is highly constrained, a number of slip systems being required to accommodate the deformation. But both the continuity of the equilibrium and of the velocity field can be satisfied alternatively by a flow in the form of a simple shear. Since the latter occupies only a tiny volume of the sample (typically  $1/10 \mu\text{m}$  in width), it is unimportant if it does not fulfil all the boundary conditions of the problem, but only the strain compatibility across the shear plane. At the beginning of a test, provided that there is no prestrain of the material,  $R$  is high and the bifurcation is not possible; but with the ongoing deformation,  $R$  drops below a threshold under which the mechanical conditions for the appearance of shear bands are met. For all the vertices, this threshold is positive, that is, shear banding is possible while the material is still work-hardening.

The planes most favoured from the point of view of  $R$  (hence, the first to allow bifurcation) have been analysed in detail. According to the crystallographic class of the vertices, they correspond to values of  $R$  ranging from 1.071 to 0.306. Although they are by no means the sole possibility of bifurcation, their geometry and the small strains at which they appear correspond to shear bands actually observed, in aluminium [20] or austenitic steel [21] for example. Nevertheless, the present theory only predicts the mechanical possibility of their onset. Hence the necessity appears to discuss the relation between the microstructural phenomena which are frequently quoted to cause shear banding and the mechanical description given above.

In the present theory, the bifurcation is seen as an abrupt change in the glide rates of the activated slip systems, without softening via damage or other alteration in the properties of the material. It is a well-established fact that even if the systems are equally favoured from the point of view of the applied stress, gliding on some of them is much more intense than on others, and that this dominance changes with the ongoing deformation [10]. This ambiguity problem has been extensively studied by Taylor from a mechanical point of view. As for metallurgical studies, they show the mechanisms through which the substructure of dislocations affects the distribution of the glide on the slip systems. For example, the Lomer dislocations, produced by the interaction of dislocations on two active

slip planes, act as an effective barrier to the dislocation movement on other (e.g. codirectional) slip systems. Such substructures are essentially instable, because of the crystalline rotations which accompany mechanical processing. Hence the changes in the distribution of the activity of the different systems.

In particular, some of them may come to a standstill while others bear the brunt of the deformation. This seems particularly important for shear banding since shear bands preferentially originate from the coarse slip due to the extensive glide on a few  $\{111\}$  planes. The combination of two coplanar or codirectional slip systems has often been observed to be the origin of shear bands [22]. What phenomena preclude other systems from working? Transmission electron microscopy puts in evidence that as deformation goes on, dislocations arrange in arrays and sometimes build up dense walls which are difficult to penetrate by the slip systems. Sometimes, this phenomenon is not directional, as in the substructure of equiaxial cells often observed in high stacking fault energy metals. But when it is, this explains that ill-oriented slip systems cannot channel through the obstacles. Two cases have been extensively documented:

- The lamellar substructures frequent in low stacking fault energy alloys. Layered dislocation walls form a periodical array of elongated subgrains. This is quite a frequent case, and it was even thought at some time to be the prerequisite to shear banding [23]. Later it was found that shear bands can superimpose on other types of dislocation arrangements.
- Similar substructures can be found in metals prone to mechanical twinning. Such is the case of copper deformed at 77K. Systematic advantage has been taken of this to provoke shear bands in order to study them [24].

All these events explain that systems may be prevented to work, while others take charge in their place, a typical pattern of bifurcation from a homogeneous, multiple slip mode of deformation.

According to KORBEL and co-workers [10], when shear bands are triggered off, they can be analysed as an ‘avalanche’ glide of dislocations, explained by the breakdown of obstacle networks. The above theory says nothing about the resistance or the collapse of such blockades, which may be, for example, the pinning of dislocations by solute atoms known as Cottrell’s atmospheres. But it shows that, for a given state of work hardening, strain and stress continuity are possible for a large range of bifurcation planes on what amounts to new, non-octahedral slip systems. It has been found that the resolved shear stress on them is somewhat higher than on the previously activated  $\{111\}\langle 110\rangle$  systems. Since the resolved critical shear stress that can be attributed to them is low, this accounts for the catastrophic character of the glide, and the almost instantaneous propagation of the shear bands.

Besides, no light is cast on the distinctive width of the localization, for which an explanation must be sought in the characteristic distance at which two dislo-

cation walls (the outer planes of the band) can attract the dislocations to leave a free channel for intense shear. Nevertheless, the above results encourage the investigation on the edges  $d = 1$ , for which experimental data are also available, as developed in the third paper of this series.

## Acknowledgment

The authors are greatly indebted to Dr. F. Montheillet, CNRS Senior Scientist, for his advice all along the development of the present project.

## References

1. M. DARRIEULAT, A. CHENAOUÏ, *Bifurcation into shear bands of the Bishop and Hill polyhedron, Part I: General analysis*, Arch. Mech., **56**, 137–156, 2004.
2. S. STÖREN, J.R. RICE, *Localized necking in thin sheets*, J. Mech. Phys. Solids, **23**, 421–441, 1975.
3. P. DUBOIS, *Etude cristallographique de l'initiation et de la propagation de bandes de cisaillement dans les métaux purs*, Ph. D. thesis, Université Paris Nord, France 1988.
4. U.F. KOCKS, G.R. CANOVA, *How many slip systems and which?* [in:] Deformation of polycrystals: mechanisms and microstructures. Invited contribution to the Second Risø Symposium on Metallurgy and Material Science, Risø, Denmark 1981.
5. G.I. TAYLOR, *Plastic strain in metals*, J. Inst. Metals, **62**, 307–324, 1938.
6. C.N. REID, *Deformation geometry for material scientists*, Pergamon Press, 162–163, Oxford 1973.
7. P. GILORMINI, B. BACROIX, J.J. JONAS, *Theoretical analyses of  $\langle 111 \rangle$  pencil glide in b.c.c. crystals*, Acta Metall., **36**, 2, 231–256, 1988.
8. M. GASPÉRINI, C. REY, *Effect of initial orientation and of predeformation on shear banding in copper single crystals submitted to tensile tests*, [in:] C. TEODOSIOU, J.L. RAPHANEL, F. SIDOROFF, Large Plastic Deformations: Fundamental Aspects and Applications to Metal Forming, Balkema, Rotterdam, 229–237, 1993.
9. R. FORTUNIER, J. LINHART, *Solid angles in  $N$  dimensional space: application of spherical volume theory to crystal yield surfaces*, Int. J. Plast., **5**, 477–499, 1989.
10. A. KORBEL, P.L. MARTIN, *Microscopic versus macroscopic aspect of shear band deformation*, Acta Metall., **34**, 10, 1905–1909, 1986.
11. S.V. HARREN, H.E. DEVE, R.J. ASARO, *Shear band formation in plane strain compression*, Acta Metall., **36**, 9, 2435–2480, 1986.
12. A.R. MOKHTARI-DOLUI, *Contribution à l'étude des bandes de cisaillement sur quelques alliages de l'aluminium*, Ph. D. thesis, Université Paris-Sud, France, 1986.
13. K.F. KARHAUSEN, J. SAVOIE, C.M. ALLEN, D. PIOT, R. LUCE, *Material testing, constitutive modeling and implementation of material models into hot rolling models for alloy AA3103*, Materials Science Forum, 396–402, 2002.

14. J.Y. POUSSARDIN, M. DARRIEULAT, *Hétérogénéités de déformation plastique dans les monocristaux d'Al 1%Mn soumis à compression plane bi-encastree*, Colloque Matériaux, Tours, France 2002.
15. M. RICHERT, A. KORBEL, *The position of shear bands in rolled f.c.c. metals*. Z. Metallkunde, 446–451, 1988.
16. Y.W. CHANG, R.J. ASARO, *An experimental study of shear localization in aluminium-copper single crystals*, Acta Metall., **29**, 241–257, 1981.
17. D.G. ATTWOOD, P.M. HAZZLEDINE, *A fiducial grid for high resolution metallography*, Metallography, **9**, 483–500, 1976.
18. D. CHAPELLE, M. DARRIEULAT, *The occurrence of shear banding in a millimetric scale  $(\bar{1}\bar{2}3)[634]$  grain of a Al-4.5Mg alloy during plane strain compression*, Mat. Sci. Eng. A, **347**, 32–41, 2003.
19. A. KORBEL, J.D. EMBURY, M. HATHERLY, P.L. MARTIN, H.W. ERBSLOTH, *Microstructural aspects of strain localization in Al-Mg alloys*, Acta Metall., **34**, 10, 1999–2009, 1986.
20. A. KORBEL, F. DOBRZAŃSKI, M. RICHERT, *Strain hardening of aluminium at high strains*, Acta Metall., **31**, 293–298, 1983.
21. W. OLIFERUK, A. KORBEL, M. GRABSKI, *Mode of deformation and the rate of energy storage during uniaxial tensile deformation of austenitic steel*, Mat. Sci. Eng. A, **220**, 123–128, 1996.
22. Z. JASIEŃSKI, A. PIĄTKOWSKI, *Nature des bandes de cisaillement macroscopiques dans les monocristaux de cuivre sollicités en compression plane*, Arch. Metall., Warszawa, **38**, 3, 279–301, 1993.
23. K. MORII, H. MECKING, Y. NAKAYAMA, *Development of shear bands in f.c.c. single crystals*, Acta Metall., **33**, 1, 379–388, 1985.
24. H. PAUL, Z. JASIEŃSKI, A. PIĄTKOWSKI, K. PAWLIK, A. LITWORA, *The influence of the 'Brass' type shear bands on the global texture of copper and CuAl2% C-oriented single crystals compressed in channel-die*, [in:] X Conference on Electron Microscopy of Solids, Warsaw-Serock, Poland, 307–312, September 20–23, 1999.

Received July 26, 2004.

---